INTERNATIONAL JOURNAL OF CLIMATOLOGY
Int. J. Climatol. **36**: 4071–4084 (2016)
Published online 25 January 2016 in Wiley Online Library
(wileyonlinelibrary.com) DOI: 10.1002/joc.4618

RMetS
Royal Meteorological Society

Prediction skill and predictability of Eurasian snow cover fraction in the NCEP Climate Forecast System version 2 reforecasts

Qiong He,[a] Zhiyan Zuo,[a]* Renhe Zhang,[a] Song Yang,[b] Wanqiu Wang,[c] Ruonan Zhang[a] and Emily E. Riddle[d]

[a] *Institute of Climate System, Chinese Academy of Meteorological Sciences, Beijing, China*
[b] *Department of Atmospheric Sciences, Sun Yat-sen University, Guangzhou, China*
[c] *Climate Prediction Center, NCEP/NWS/NOAA, College Park, MD, USA*
[d] *Department of Geosciences, University of Massachusetts, Amherst, MA, USA*

ABSTRACT: Eurasian snow cover fraction (SCF) prediction is analyzed using the recently developed National Centers for Environmental Prediction (NCEP) Climate Forecast System version 2 (CFSv2) monthly retrospective forecasts for 1983–2009. The CFSv2 is generally capable of reproducing the observed Eurasian SCF seasonal cycle and climatology. This study focuses on the prediction skill and predictability of Eurasian SCF in snowmelt and snowfall seasons because the intensive variability occurs in the two seasons. The CFSv2 reasonably predicts the interannual variations, long-term trend and leading pattern in snowmelt season several months ahead. In comparison with the snowmelt season, the CFSv2 shows a better prediction skill in climatological values but a worse skill in the interannual variability in snowfall season. In addition, the forecasted downward trend of SCF in the snowfall season is opposite to that in the observation. The biases of Eurasian SCF in the snowmelt and snowfall seasons are significantly related with those of temperature and precipitation in the CFSv2. The forecasted cooler and wetter atmosphere is suggestive of the overestimation of the mean SCF. Meanwhile, the underestimation in the variability of both temperature and precipitation in the CFSv2 may be the important factor for the underestimated variability of SCF, especially for the damped variability of SCF in the snowfall season. Generally, the CFSv2 shows a higher and more stable prediction skill after late-1990s than before in the two seasons. The change in the initial condition in the CFSv2 and the observed SCF in late-1990s might be the plausible reason for it.

KEY WORDS snow cover fraction; NCEP CFSv2; prediction; predictability

Received 23 August 2015; Revised 24 November 2015; Accepted 25 November 2015

1. Introduction

Snow is an important element having dramatic effect on the climatic and hydrologic models, atmospheric circulation patterns and global heat budget (Barnett *et al.*, 1989; Clark *et al.*, 1999; Clark and Serreze, 2000; Singh *et al.*, 2007; Brands *et al.*, 2012; Zuo *et al.*, 2012a; Chen *et al.*, 2013; Orsolini *et al.*, 2013; Zuo *et al.*, 2014). For example, Gong *et al.* (2003) reported that Eurasian snow cover in October plays an important role on the large-scale atmospheric circulation in mid- and high-latitude through influencing the interactivity between troposphere and stratosphere. Cohen and Jones (2011) suggested that the interaction between snow cover and atmosphere can affect the fundamental climate in winter and snow cover can be considered as a good predictor for seasonal climate prediction. Wu and Kirtman (2007) and Zuo *et al.* (2012b) reported that the decreasing Eurasian snow cover in spring is significantly associated with the synchronic reducing precipitation in southeastern China. Zhang *et al.* (2008, 2013) and Wu *et al.* (2009) showed that the spring snow cover over Eurasian continent had major impact on the decadal variability of summer rainfall over eastern China.

It is vital for climate models to precisely simulate the snow process. Recently, the development of coupled ocean–atmosphere model prediction systems has made great progress in seasonal climate predictions (Kumar *et al.*, 2005; Wang *et al.*, 2005; Kug *et al.*, 2008; Mo *et al.*, 2012). The National Centers for Environmental Prediction (NCEP) Climate Forecast System version 2 (CFSv2), successor of the first CFS, was made operational at NCEP in March 2011 (Saha *et al.*, 2014). The predictive skills of the CFSv2 in Madden–Julian Oscillation, El Niño Southern Oscillation, the tropical Atlantic SST, the Artic Oscillation and in monsoon precipitation, surface air temperature and sea ice have been assessed in previous studies (Kim *et al.*, 2012; Wang *et al.*, 2012; Peng *et al.*, 2013; Riddle *et al.*, 2013; Wang *et al.*, 2013; Zuo *et al.*, 2013; Hu and Kumar, 2014; Saha *et al.*, 2014). With the upgraded four level soil model used in the CFSv2 system (Saha *et al.*,

* Correspondence to: Z. Zuo, Institute of Climate System, Chinese Academy of Meteorological Sciences, No. 46, Zhongguancun South Street, Beijing 100081, China. E-mail: zyzuo@camscma.cn

© 2016 The Authors. *International Journal of Climatology* published by John Wiley & Sons Ltd on behalf of the Royal Meteorological Society. This is an open access article under the terms of the Creative Commons Attribution-NonCommercial-NoDerivs License, which permits use and distribution in any medium, provided the original work is properly cited, the use is non-commercial and no modifications or adaptations are made.

2013), Zuo *et al.* (2011, 2013) suggested that the CFSv2 is able to simulate some dynamical processes associated with snow cover. Nevertheless, the detail predictive skill of the CFSv2 in the Eurasian snow cover still needs to be further documented. In this study, we evaluate the prediction skill and predictability of the Eurasian snow cover fraction (SCF) in the NCEP CFSv2 reforecasts. Considering the small variability of the Eurasian SCF during all winter months and little snow cover during summer, this study primarily focuses on the prediction and predictability of Eurasian SCF in snowmelt and snowfall seasons. The paper is organized as follows: Section 2 briefly describes the CFSv2 reforecasts and observational datasets, as well as the analysis method. Section 3 presents the general predictive skill and predictability of Eurasian SCF. Section 4 focuses on the predictive skill in the snowmelt season and Section 5 focuses on the snowfall season. Section 6 examines the possible causes for the CFSv2 prediction skill. Summary and discussion are provided in Section 7.

2. Model, data and methods

The CFSv2 is a fully coupled model which consists of the NCEP Global Forecast System atmospheric model, Modular Ocean Model version 4 from Geophysical Fluid Dynamics Laboratory, an interactive three sea ice model and Noah land surface model (Saha *et al.*, 2014). The retrospective 9-month forecasts of the CFSv2 have initial condition (IC) of the 0, 6, 12, 18Z cycles for every 5 days, starting from 1 January 0Z of every year for 1982–2010. This study uses 16 members with 0–8 lead-month (LM) (i.e. 0, 6, 12, 18Z on 12, 17, 22, 27 March for April prediction for LM0) from the CFSv2 9-month retrospective SCF (1983–2009) to analyze the prediction skill and predictability of the Eurasian snow cover. The SCF in the CFSv2 is derived from the simulated snow depth and is related with the surface characteristics and snowpack density (Ek *et al.*, 2003). Also, the 850 hPa, 2-m temperature and surface precipitation rate from the CFSv2 reforecasts are used in the analysis of possible causes for the SCF prediction. The LM0 is referred to as initialized from its previous month. The IC of the CFSv2 reforecasts is provided by the NCEP Climate Forecast System Reanalysis (CFSR), which has been proven superior to the previous NCEP reanalyses (Saha *et al.*, 2010).

We use the satellite-based SCF dataset provided by the Rutgers Global Snow Lab to evaluate the prediction of Eurasian SCF in the CFSv2. The monthly SCF in the Rutgers Global Snow Lab is based on the weekly satellite-derived snow cover maps produced weekly by trained National Oceanic and Atmospheric Administration (NOAA) meteorologists for 1966–1997 (Robinson *et al.*, 1993). From 1997 to present, it is changed to base on the NOAA Ice and Snow Mapping System (IMS) daily snow charts, with a higher temporal and spatial resolution (Ramsay, 1998). In addition, the air temperature at 850 hPa from the ERA-Interim and 2-m air temperature from the Climate Precipitation Center monthly land surface air temperature observations are used to evaluate the prediction of atmospheric temperature (Fan and van den Dool, 2008; Berrisford *et al.*, 2009). Global Precipitation Climatology Project (GPCP) version 2.2 monthly precipitation dataset (Adler *et al.*, 2003), which consists of precipitation derived from satellite and gauge measurements, is also used as the validation dataset.

The methods in this study include anomaly correlation coefficient (ACC), root-mean-square error (RMSE) and spatial correlation. The non-parametric Mann–Kendall test (Mann, 1945 and Kendall, 1975) is used to detect significant trend in the time series of spatial correlation. In addition, the maximized signal-to-noise ratio empirical orthogonal function analysis (MSN EOF) is used to isolate the most predictable patterns by maximizing the ratio of the variances of the ensemble mean and within-ensemble deviations (Venzke *et al.*, 1999; Huang, 2004; Zuo *et al.*, 2013).

3. General prediction skill

We first analyze the general prediction skill and predictability of Eurasian SCF in the CFSv2. Figure 1(a) exhibits the observed climatological month-to-month changes of SCF. The positive (negative) value in each month represents that the snow-accumulation (snow-ablation) process is dominant during this month. Thus, September–January refers snowfall months whereas February–August refers snowmelt months. We further define the months with month-to-month absolute change value exceeding 10 (unit: %) as snowmelt/snowfall season. April–June and October–December represents snowmelt and snowfall season, respectively. Generally, Eurasian snow starts to accumulate during October, with substantial increase during October–December. Then snow reaches peak and keeps relative stable with maximum in winter. From April on, snow decreases rapidly, resulting in little snow cover during June–September over Eurasia. Figure 1(b) illustrates the seasonal cycle of Eurasian SCF in the observation and CFSv2 for LM0-8. The CFSv2 captures the seasonal cycle of Eurasian SCF reasonably. The CFSv2 for LM0 reproduces the observed SCF climatology in February–April and July–August quite well, but a little larger in September–October and smaller in November–January and May–June. For longer LMs, the CFSv2 shows different prediction skills, with general less-than-observed SCF in November–January and more-than-observed SCF in April–June and September–October. The spread of model value tends to be greater in snowmelt season than in snowfall season.

Figure 2 shows the ACC and RMSE for LM0-8 as a function of target month and LM. The dash line in Figure 2(a) is the contour exceeding the 95% confidence level (Student's *t*-test). It is found that the ACC in snowmelt months (February–July) is generally significant for shorter than LM6. In contrast, the ACC in snowfall months (September–January) is much smaller for all

© 2016 The Authors. *International Journal of Climatology* published by John Wiley & Sons Ltd on behalf of the Royal Meteorological Society.

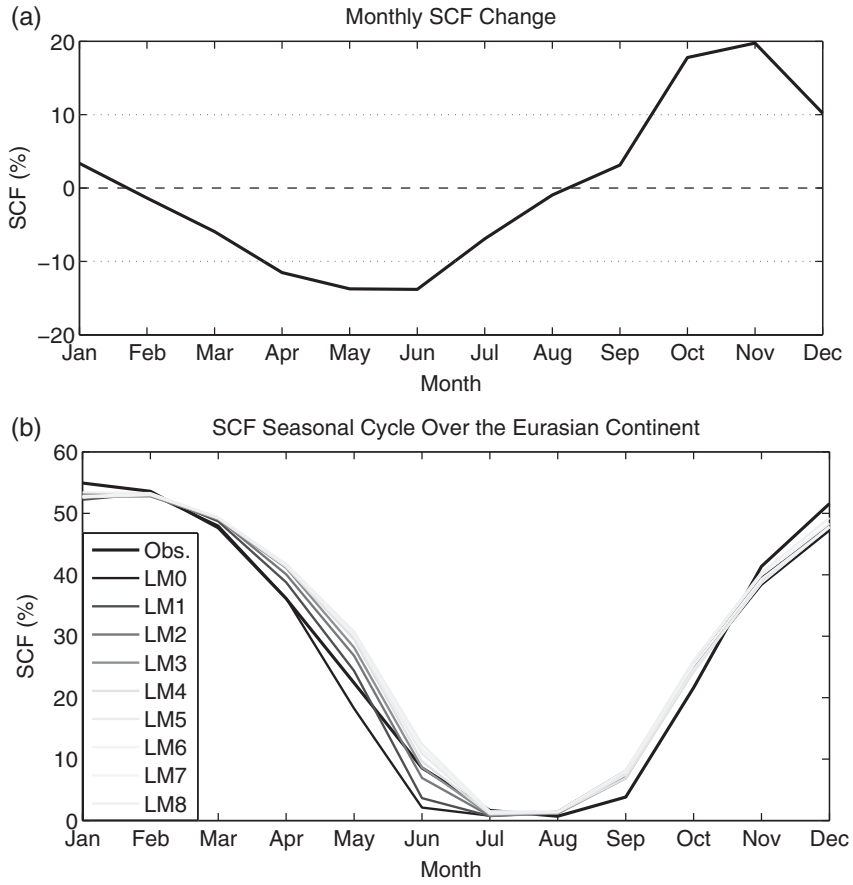

Figure 1. (a) Monthly climatological SCF change (the value of month n refers SCF of month n minus n-1). (b) Climatological SCF in the observation (black) and CFSv2 forecasts for LM0-8 (coloured curves).

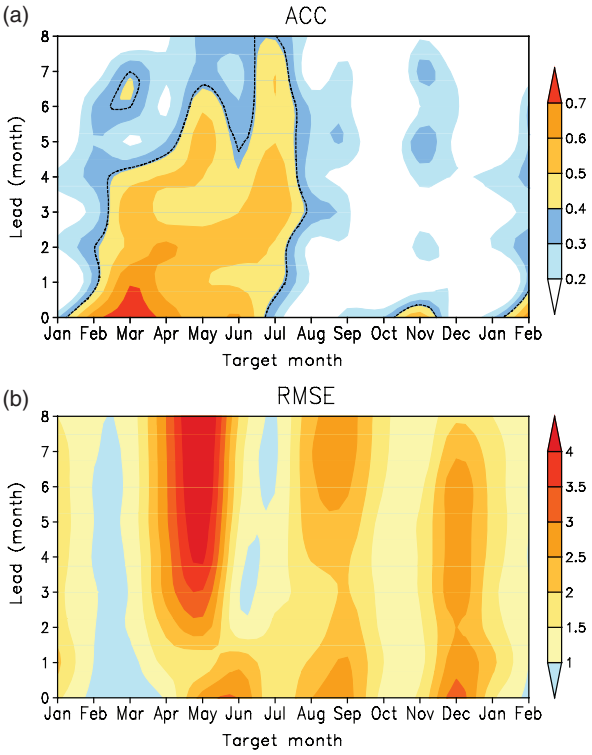

Figure 2. (a) SCF ACC and (b) RMSE (unit: %) between the observation and CFSv2 forecasts as a function of target month and LM.

LMs. The RMSE in major snowmelt months (April–June) varies intensively with LMs and is relatively larger than that in other months. Overall, the CFSv2 exhibits better predictable skill in the SCF variations but larger bias and spread in climatological value in snowmelt months than in the snowfall months.

The intensive SCF variation generally occurs in the snowmelt and snowfall seasons and the characteristics of SCF in the two seasons are quite different. Hereafter, we primarily focus on the SCF prediction skill in the two seasons, represented by April and October since the beginning of extensive snow ablation and accumulation generally occurs in April and October, respectively.

4. Eurasian SCF prediction and predictability in snowmelt season

Figure 3 shows the observed climatology of Eurasian SCF and its differences with the CFSv2 for LM0, LM2 and LM5 in April (model-observation). As expected, the SCF increases from south to north, with maximum gradient in 30°–140°E, 45°–65°N. The SCF is greater than 75% in north of 60°N and less than 25% in south of 50°N except Tibetan Plateau (TP). Generally, the CFSv2 predicts the climatological Eurasian SCF with positive biases in the northeast of China and negative biases in north of TP.

© 2016 The Authors. *International Journal of Climatology* published by John Wiley & Sons Ltd on behalf of the Royal Meteorological Society.

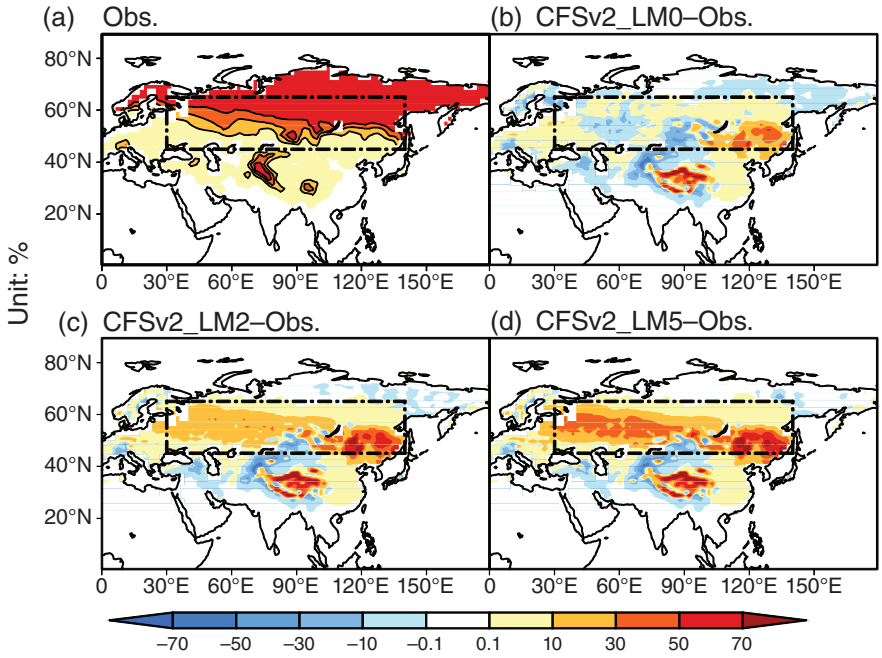

Figure 3. The mean April SCF (%) during 1983–2009 from (a) Rutgers observation (solid line shows contours of 25, 50 and 75%) and climatological biases in April SCF (model-observation, unit: %) for (b) LM0, (c) LM2 and (d) LM5. The black dashed rectangles in (a)–(d) represent region of 30°–140°E, 45°–65°N defined as SMKA.

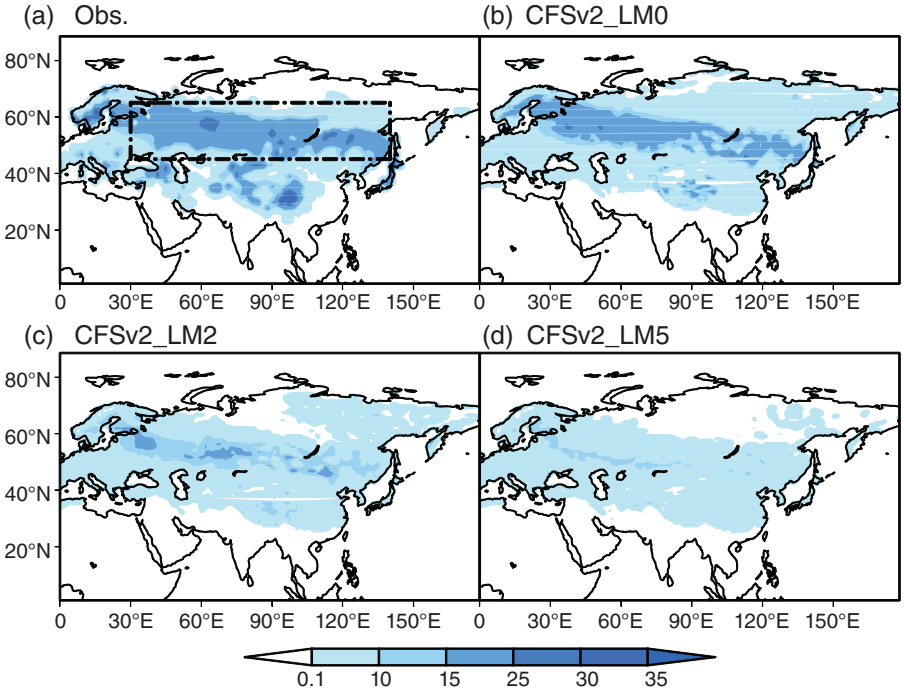

Figure 4. Standard deviation of April SCF for (a) Rutgers observation and CFSv2 for (b) LM0, (c) LM2 and (d) LM5. The black dashed rectangle in (a) is the same as Figure 3.

Over the high latitude of Eurasia about north of 65°N, the biases are quite small and vary little with LMs because of the SCF is always nearly 100%. Noted that these biases in the domain with maximum gradient (30°–140°E, 45°–65°N) increase significantly with LMs, which is consistent with Figure 1(b). In the study, we do not investigate the prediction and predictability in TP because of the poor quality of the observed SCF dataset here.

The standard deviation of the SCF in the observation and CFSv2 for different LMs is calculated to evaluate the predictive skill in the SCF variability (Figure 4). The maximum variability, greater than 15%, is located in 30°–140°E, 45°–65°N where the gradient are largest (Figures 3(a) and 4(a)) in the observation. The CFSv2 for LM0 shows similar pattern to the observation with maximum variability in 30°–140°E, 45°–65°N, but with

© 2016 The Authors. *International Journal of Climatology* published by John Wiley & Sons Ltd on behalf of the Royal Meteorological Society.

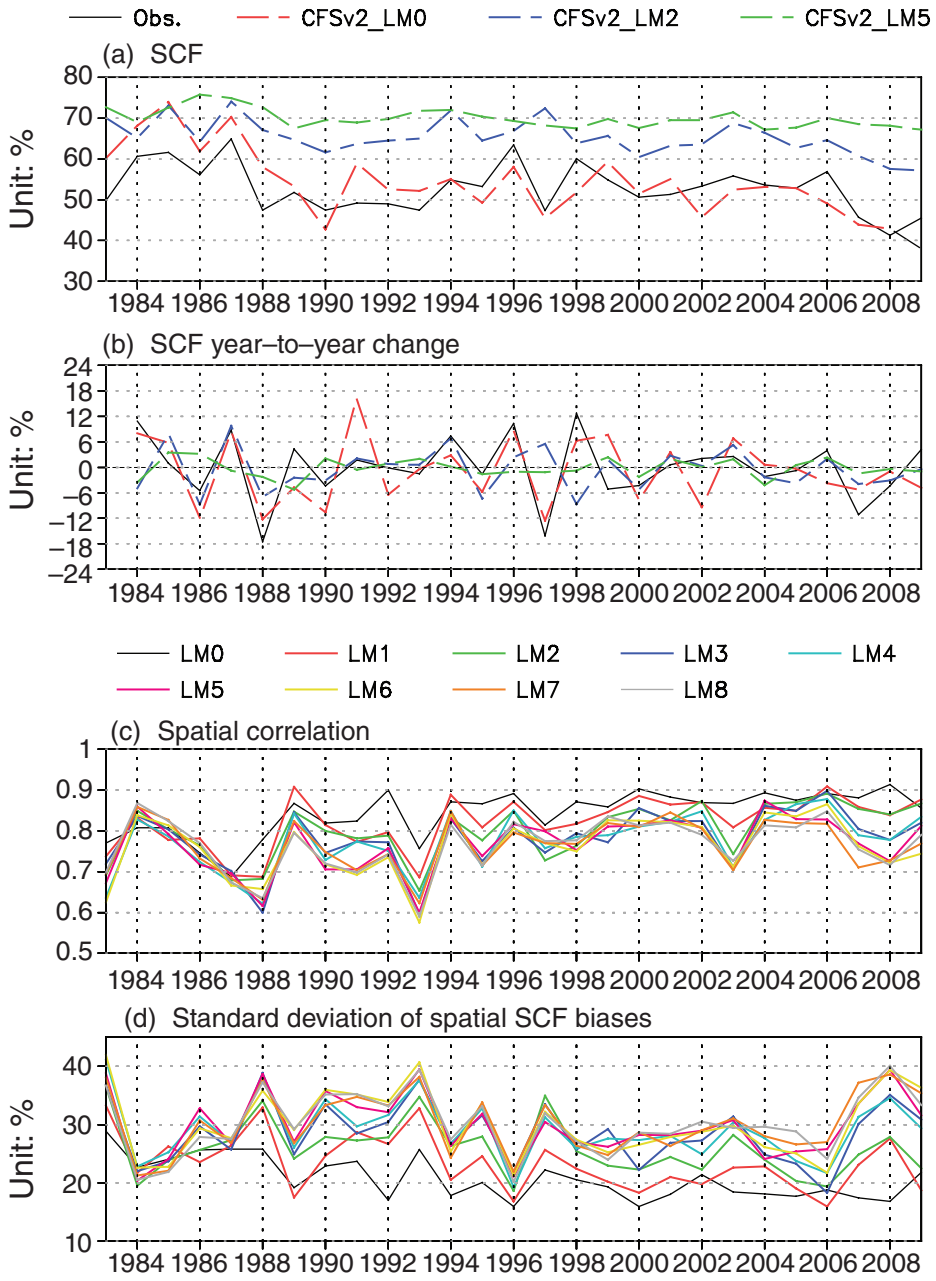

Figure 5. Observed and forecasted (a) SCF and (b) year-to-year SCF variation (the value of year n refers SCF of year $n - n - 1$) averaged over SMKA in April. The unit is %. (c) Time series of spatial correlation between CFSv2 for LM0-8 and the observation in April. (d) Time series of standard deviation of spatial SCF biases between CFSv2 for LM0-8 and the observation in April. Unit: %.

a little smaller magnitude. For longer LMs, the SCF variations decrease rapidly, with the value greater than 15% over some sporadic small areas in East Europe Plain and south of Baikal for LM2 and less than 10% in most parts of Eurasia for LM5.

As aforementioned, both the most intensive snowmelt and model bias are located over 30°–140°E, 45°–65°N (the domain with black dashed rectangles in Figure 3, 4). Thus, we define this area as snowmelt key area (SMKA) representing the whole Eurasia to further study the predictive skill in the SCF interannual variability in snowmelt season. Figure 5(a) shows the time series of April SMKA SCF in the CFSv2 and observation. The CFSv2 for LM0 predicts the similar interannual variability and climatological value to the observation. For longer LMs, the CFSv2 gradually exaggerates the SMKA SCF climatological value while underestimates the interannual variability. Nevertheless, all the ACCs in the SMKA SCF between the observation and CFSv2 reforecasts for LM0-4 are significant ($R = 0.70$, 0.52, 0.55, 0.42, 0.53, respectively, exceeding the 95% confidence level). Namely, the CFSv2 is capable of forecasting the interannual variation 5 months in advance despite the weaker-than-observed intensity of variation for the LMs longer than LM2 (also seen in Figure 12(b)).

The observation shows a downward trend (-0.25% year^{-1}) in April SCF and the CFSv2 for all

© 2016 The Authors. *International Journal of Climatology* published by John Wiley & Sons Ltd on behalf of the Royal Meteorological Society.

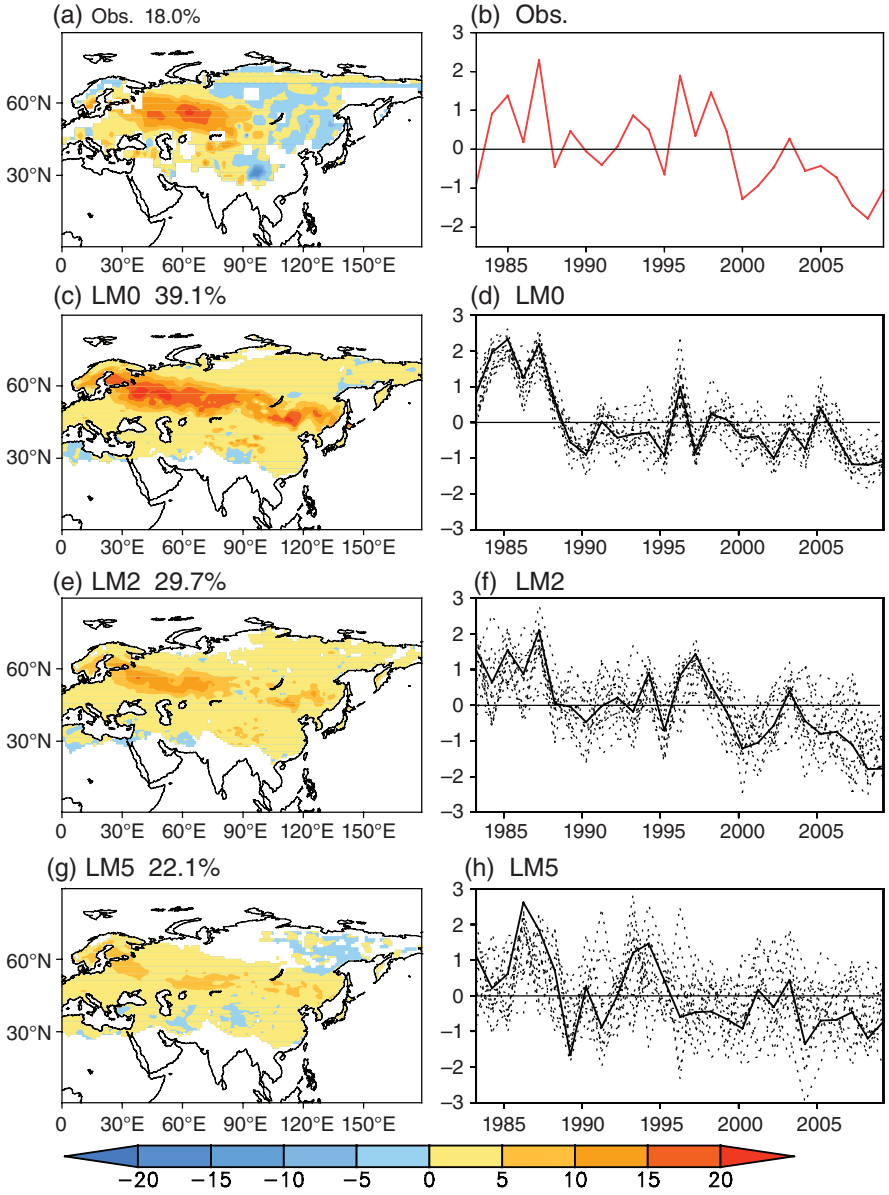

Figure 6. (a) First EOF mode of SCF (%) in the observation (a) and the first MSN EOF mode of CFSv2 forecasts over Eurasia in April for (c) LM0, (e) LM2 and (g) LM5. PC1 in the observation (b) and PC1s in the CFSv2 for (d) LM0, (f) LM2 and (h) LM5. The solid black lines and dashed lines in (d), (f) and (h) are the PC1s of the ensemble means and individual members, respectively.

LMs captures the trend well, except with stronger amplitude for LM0-1 (−0.76/−0.51% year^{-1} for LM0/1). This may be related with the robust decreasing trend of the IC (−0.57% and −0.39 year^{-1} for March and February, respectively in the CFSR). For longer LMs, the forecasted downward trends become moderate and gradually close to the observation.

To further assess the interannual variation, we calculate the year-to-year (Y2Y) variation (Figure 5(b)). The CFSv2 is generally capable of forecasting the Y2Y variation for LM0-1 (correlation coefficient of 0.59 and 0.40) but unable to forecast it for longer LMs. The predictive skill varies with the year. For example, the forecasted Y2Y variation is relatively realistic in 1986–1988 for LM0-2, but it shows opposite anomalies to the observation in 1989 and 1999 even for LM0. In order to estimate the dependence of predictive skill on years, we analyze the spatial correlation between the observation and CFSv2 for LM0-8 (Figure 5(c)). The spatial correlation coefficients differ from each year with relatively greater value and weaker fluctuation after late-1990s, which has been verified with the M–K test (not shown), indicating that the prediction skill has been improved after late-1990s. In addition, the time series of standard deviation of spatial SCF biases also exhibit a relative low value after the late-1990s in comparison with before, further justifying the improvement of prediction skill after late-1990s.

Figure 6(a) and (b) illustrate the leading EOF spatial pattern and corresponding principal component (PC1) of Eurasian April SCF in the observation. The prominent feature in the EOF1 pattern is the intensive variation in western Siberia (the maximum value greater than

© 2016 The Authors. *International Journal of Climatology* published by John Wiley & Sons Ltd on behalf of the Royal Meteorological Society.

20%) and the obvious decreasing trend in the PC1. Figure 6(c)–(h) exhibit the leading MSN EOF patterns and corresponding PC1s of Eurasian SCF in the CFSv2 for LM0, LM2 and LM5. The leading predictable pattern of CFSv2 for LM0 captures the vigorous variability in western Siberia and the decreasing trend in the observed PC1. The relationship between the PC1s of the observation and the CFSv2 ensemble mean for LM0 is significant ($R = 0.67$, seen in Table 1). In addition, the spreads among the members are quite small and all the 16 members show significant correlation with the observation (Figure 6(d)). The CFSv2 for LM2 also predicts the robust variation in western Siberia although the magnitude is a little smaller than that in the observation (Figure 6(e) and (f)). Furthermore, all the correlation coefficients between the PC1 in the observation and the PC1s of the ensemble mean and 12 of 16 members exceed the 95% confidence level, indicating that the CFSv2 for LM2 generally reproduces the variation in the observation (Table 1). Moreover, the correlation between the year-to-year PC1s of the observation and CFSv2 ensemble means for LM0 and LM2 is also significant (exceeding the 99% confidence level), indicating a good predictive skill of the CFSv2 in the interannual variations of the leading pattern of SCF in April for 3 months ahead. In addition, the CFSv2 does not reproduce the moderate negative anomalies around eastern Siberia in the observation for LM0 and LM2. For longer LMs, the pattern biases between the CFSv2 and observation and the spreads among the 16 members become considerable. The intensive variation in western Siberia generally disappears in the CFSv2 for LM5 and neither of the ensemble mean nor any members show significant relationship with the observation in the PC1 (Figure 6(g) and (h)). The spreads among the 16 members for LM5 are also quite large. Overall, the CFSv2 can predict the leading pattern of Eurasian SCF 3 months in advance. After 3 months, it shows poor prediction and predictability in Eurasian SCF leading pattern.

Table 1. Correlation coefficients between the observed PC1 and forecasted PC1s of the ensemble mean (the second column) and 16 ensemble members (the other columns) in the CFSv2 for LM0 (top), LM2 (middle) and LM5 (bottom) in April.

LM	Mean	16 members							
LM0	**0.67**	**0.65**	**0.67**	**0.67**	**0.72**	**0.55**	**0.59**	**0.57**	**0.56**
		0.62	**0.63**	**0.49**	**0.48**	**0.75**	**0.65**	**0.58**	**0.56**
LM2	**0.76**	**0.7**	**0.51**	**0.5**	**0.57**	**0.62**	**0.49**	0.37	**0.7**
		0.35	**0.69**	0.47	**0.66**	0.48	**0.64**	**0.53**	**0.65**
LM5	0.36	0.3	−0.01	0.22	0.06	0.08	0.11	0.12	0.01
		0.1	0.13	0.17	0.4	0.15	**0.43**	0.34	0.4

Bold numbers are above the 99% confidence level (Student's *t*-test).

5. Eurasian SCF prediction and predictability in snowfall season

Figures 7 and 8 demonstrate the climatology and standard deviation of Eurasian SCF in October in the observation and its differences with the CFSv2 for LM0, LM2 and LM5. As expected, the large SCF in the observation is found in the high latitudes. The SCF, greater than 25%, extends from north of 65°N southward to near 60°N in October, with more than 75% in north of 65°N whereas less than 25% in south of 60°N except the TP. The region with large SCF gradient, 30°–140°E, 50°–70°N, is also with high standard deviation (greater than 25%; Figures 7(a) and 8(a)). The homogeneous positive biases of the SCF in October, with the maximum greater than 10%, are also located in the region with large gradient and variability,

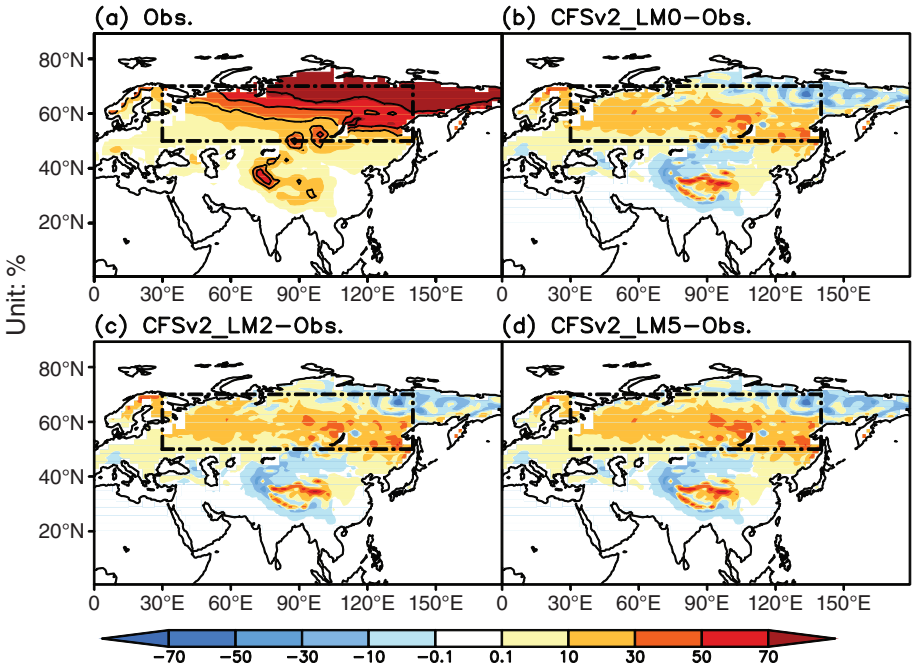

Figure 7. Same as Figure 3, but for October. The black dashed rectangle in (a)–(d) represent region of 30°–140°E, 50°–70°N defined as SFKA.

© 2016 The Authors. *International Journal of Climatology* published by John Wiley & Sons Ltd on behalf of the Royal Meteorological Society.

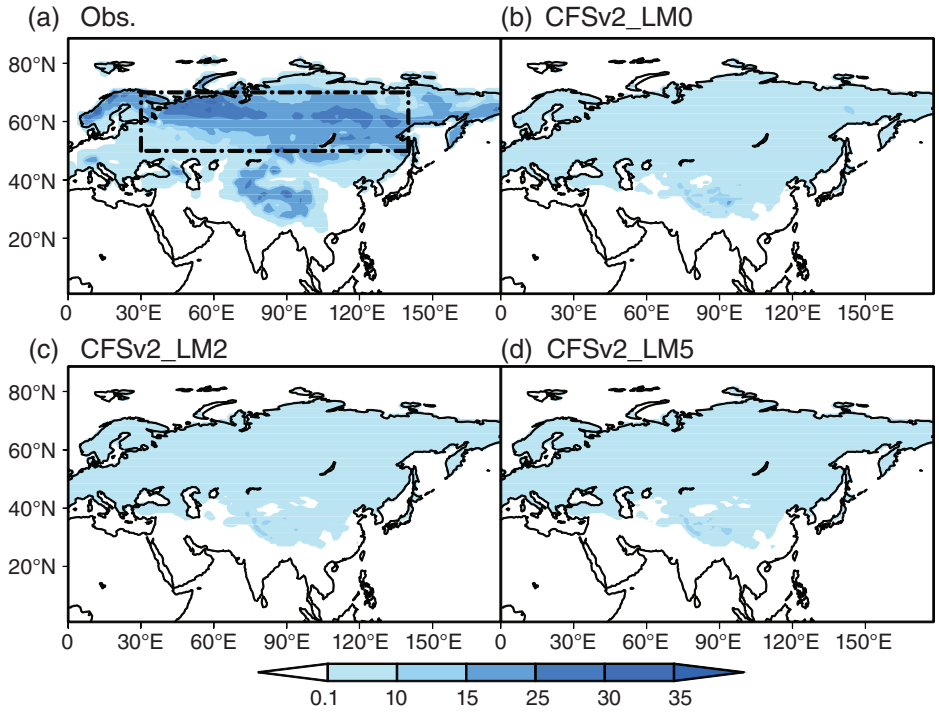

Figure 8. Same as Figure 4, but for October. The black dashed rectangle in (a) is the same as Figure 7.

same as the condition in April. However, it is different from April (Figures 7(b)–(d), 3(b)–(d)) that the biases vary little as the LM increases. The observed standard deviations over 30°–140°E, 50°–70°N are generally greater than 25%. The CFSv2 for all of the LMs cannot predict this large variation (Figure 8 (b)–(d)). As aforementioned, we do not discuss the large biases around the TP.

Similarly, we define the area (30°–140°E, 50°–70°N) with vigorous gradient, variability and bias as the snowfall key area (SFKA). The time series of the SFKA SCF in the observation and CFSv2 for LM0, LM2 and LM5 in October are shown in Figure 9(a). The observed SFKA SCF displays an obvious uptrend with linear trend of 0.73% year^{-1}. However, the CFSv2 shows a weak downtrend (−0.06, −0.10 and −0.10% year^{-1} for LM0, LM2 and LM5, respectively), incapable of reproducing the observed uptrend. The reason for the discrepancy is not clear and it will be discussed in Section 7.

The interannual variations in the CFSv2 are much weaker than those in the observation (Figure 9(a)). The causes for the weak variability might come from the much weaker variability of October precipitation and temperature (further discuss about it in Section 6). Actually, previous studies reported that the weaker-than-observed variation of SCF is common phenomenon in most numerical models (Hardiman *et al.*, 2008; Riddle *et al.*, 2013). With the forecasted opposite trend and damped variability, the CFSv2 shows insignificant relationship with the observed SFKA SCF for all LMs. Nevertheless, the correlation coefficient between the detrended/Y2Y SFKA SCF in the CFSv2 for LM0 and the observation is significant ($R = 0.44/0.50$, exceeding the 95% confidence level). This feature suggests the probably predictive skill in the interannual variation. Figure 9(c)–(d) displays the time series of spatial correlation coefficients and standard deviation of spatial SCF biases. Same as in April, the CFSv2 exhibits higher and more stable prediction and predictability after late-1990s. We will discuss the phenomenon in Section 7.

Figure 10 illustrates the EOF1 of Eurasian October SCF in the observation and the MSN EOF1 in the CFSv2 for LM0, LM2 and LM5 and their corresponding PC1s. The observed Eurasian SCF exhibits homogenous variation over most parts of Eurasia, with the maximum value greater than 15% over SFKA (Figure 10(a)). The CFSv2 simulates the similar pattern with the observation but with much weaker magnitude even for LM0 (Figure 10(c), (e) and (g)). The PC1 in the observation exhibits an obvious upward trend, whereas none of the PC1s in the CFSv2 for LM0, LM2 and LM5 reproduce it successfully. In addition, all the correlation coefficients between the PC1s of the observation and CFSv2 are insignificant and the spreads among the 16 members in October are much larger than that in April (Figure 6(d), (f) and (h)). Overall, in contrast with the snowmelt season, the CFSv2 shows a better predictive skill in the climatology but a worse predictive skill and predictability in the trend, interannual variation and variability of Eurasian SCF in snowfall season.

6. Plausible causes for the prediction and predictability

As described above, the CFSv2 is able to predict the Eurasian SCF interannual variation in April ahead of several months whereas it fails to simulate that in October. Because the temperature and precipitation affect snow

© 2016 The Authors. *International Journal of Climatology* published by John Wiley & Sons Ltd on behalf of the Royal Meteorological Society.

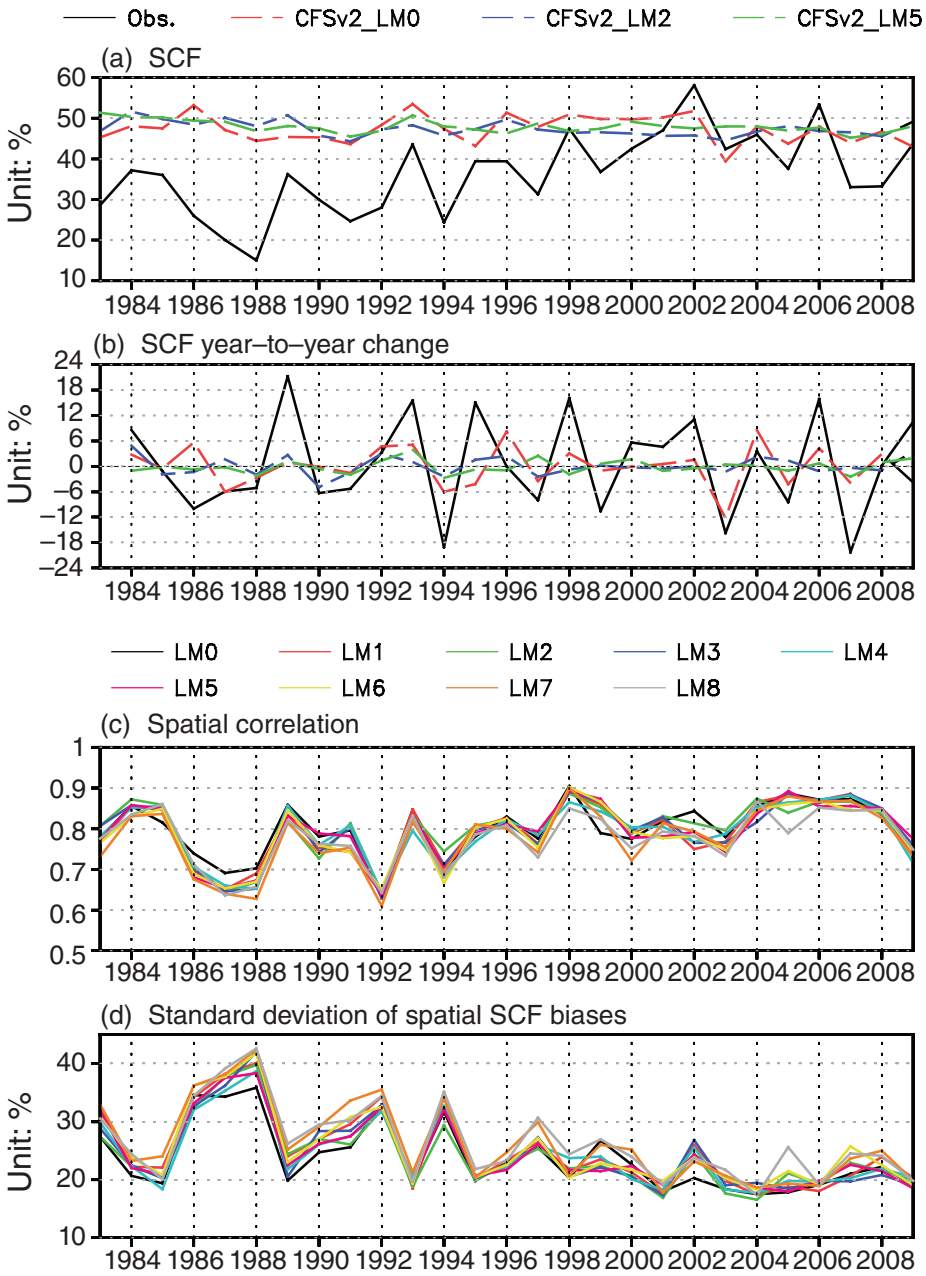

Figure 9. Same as Figure 5, but for October.

accumulation and ablation (Koren *et al.*, 1999), we attempt to explain these SCF biases by evaluating the simulation for low tropospheric temperature (LTT) and precipitation in the CFSv2. We mainly focus on the correlation between their biases and comparison of their climatological value and variability.

Figure 11 shows the correlation coefficients of the SCF biases with precipitation, 2-m temperature (T2m) and 850 hPa temperature (T850) biases in the CFSv2 for LM0 in April and October. In April, the SCF biases exhibit significant negative relationship with the forecasted LTT biases over large parts of SMKA (Figure 11(c) and (e)). In comparison, the relationship with precipitation biases is much weaker. From Figure 11(a), the significant correlation only appears over some sporadic parts of the SMKA. In October, both the biases of LTT and precipitation have significant relationship with the SCF biases (Figure 11(b), (d) and (f)). In addition, the SCF biases for longer LMs show similar relationship with the precipitation and LTT biases (figure not shown). These features suggest that the prediction and predictability of April SCF in the CFSv2 is primarily related to the predictive skill in LTT whereas the predictive skill in October SCF is associated with both the LTT and precipitation. It confirms the results of other studies that the model accumulates snow during precipitation events with surface temperature below freezing whereas it melts snow mostly dependent on the surface temperature (Frei *et al.*, 2003). We also demonstrate that the prediction skill of LTT is greater than precipitation in the CFSv2. As shown in Table 2,

© 2016 The Authors. *International Journal of Climatology* published by John Wiley & Sons Ltd on behalf of the Royal Meteorological Society.

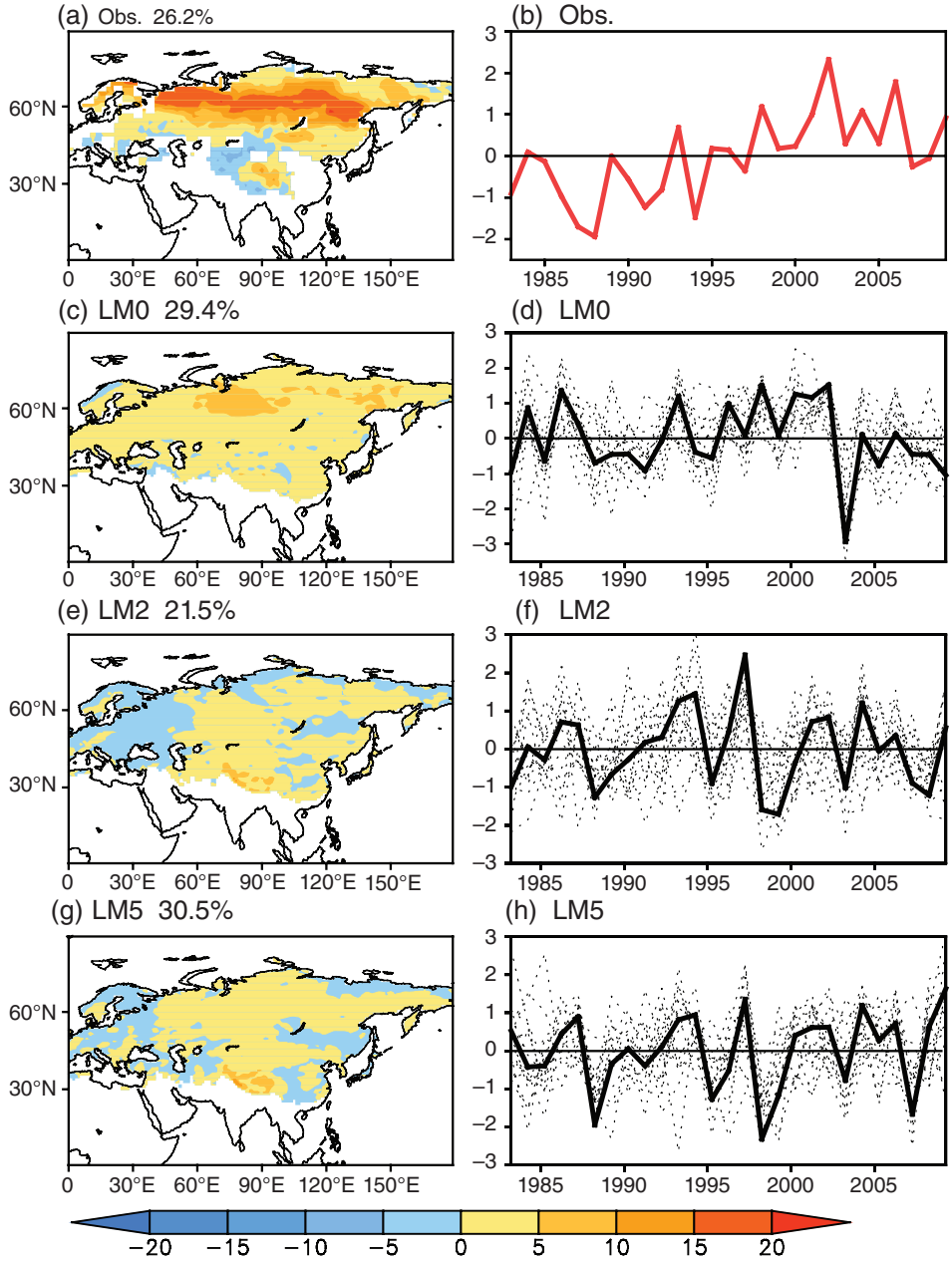

Figure 10. Same as Figure 6, but for October.

the correlation coefficients between the observation and CFSv2 for LM0-8 of T2m and T850 are generally larger than precipitation. It is capable of forecasting the LTT interannual variation ahead of 2 months while it fails to simulate that of precipitation. Overall, the poor prediction skill for precipitation and its close relationship with October SCF may interpret the worse prediction skill in the interannual variability of SCF in October than in April.

We further investigate the biases of the SCF, precipitation, T2m and T850 over SMKA in April and over SFKA in October (Figure 12). The CFSv2 produces cooler and wetter atmosphere in the CFSv2, which prevents from snowmelt but conduces to snow accumulation, corresponding to the overestimation of SCF in both seasons (Figure 12(a)). The negative biases of LTT and positive biases of precipitation in April is much larger than those in October, which could interpret the general larger biases of SCF in April. Because the SCF biases show a more significant relationship with the LTT biases than with the precipitation biases in April, the more dominant effect of temperature than the precipitation is accompanied by the gradually larger SCF biases with longer LMs (black bars in Figure 12(a)). In October, the biases of SCF exhibit a decrease from LM1 to LM4 and an increase with longer LMs for LM5–LM8, which is consistent with the evolution of LTT biases (gray bars in Figure 12(a), (e), (g)). On the other hand, the forecasted standard deviation biases of LTT and precipitation are generally negative (Figure 12(d), (f) and (h)) in both seasons, which are consistent with the underestimated SCF variability in the CFSv2 (Figure 12(b)). Noted that the underestimation of precipitation variability in October is worse than in April

© 2016 The Authors. *International Journal of Climatology* published by John Wiley & Sons Ltd on behalf of the Royal Meteorological Society.

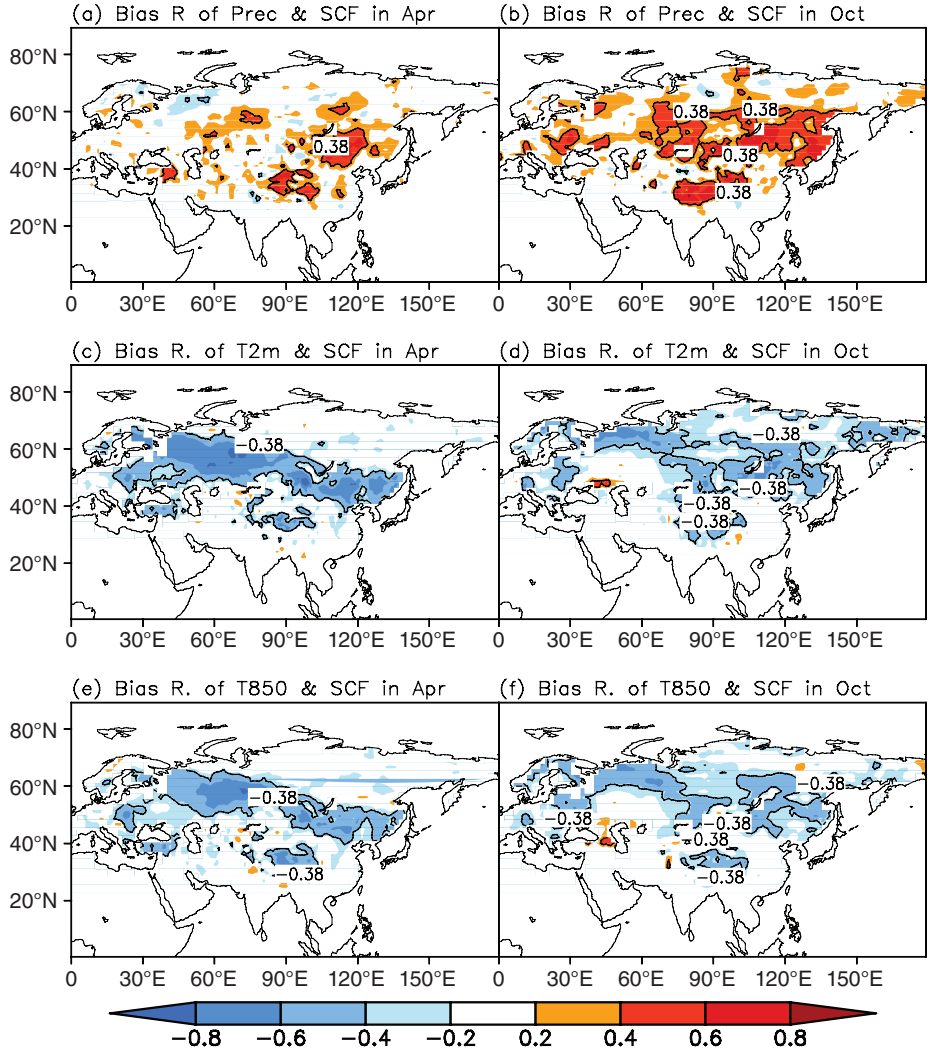

Figure 11. Correlation coefficients between SCF biases and precipitation (a, b), 2-m temperature (c, d) and 850 hPa temperature (e, f) biases of CFSv2 for LM0 in April (a, c, e) and October (b, d, f). The bold black line is the contour exceeding the 95% confidence level (Student's *t*-test).

Table 2. Correlation coefficients between forecasted and observed precipitation, T2m and T850 in April and October for LM0-8.

		LM0	LM1	LM2	LM3	LM4	LM5	LM6	LM7	LM8
April	Prc	0.03	0.20	0.07	0.11	0.16	0.19	0.12	0.03	−0.01
	T2m	**0.58**	**0.50**	0.23	0.27	0.34	0.23	0.21	0.14	0.09
	T850	**0.57**	**0.44**	0.14	0.24	0.30	0.17	0.17	0.09	0.09
October	Prc	−0.02	−0.06	0.10	−0.20	0.25	0.25	0.22	−0.32	0.42
	T2m	**0.63**	**0.38**	0.20	0.18	0.23	0.36	0.19	0.24	0.27
	T850	**0.60**	0.34	0.20	0.15	0.29	0.43	0.15	0.26	0.05

Bold numbers are above the 95% confidence level (Student's *t*-test).

(Figure 12(d)), which probably causes the worse underestimation of October SCF interannual variability than April SCF (Figure 12(b)).

7. Summary and discussion

In this study, the prediction and predictability of Eurasian SCF in terms of climatology, the temporal–spatial variation in snowmelt and snowfall season has been assessed using the CFSv2 reforecasts. The CFSv2 reasonably reproduces the seasonal cycle and climatology of the observed Eurasia SCF, with positive biases in April–October and negative biases in November–February. Because the intensive variability generally occurs in the snowmelt and snowfall seasons, this study focuses on the prediction and predictability of Eurasian SCF in the two seasons.

In the snowmelt season, the CFSv2 is generally able to predict the interannual variability, long-term trend and leading pattern of Eurasian SCF ahead of 3 months. For longer LMs, the biases of SCF in the SFKA increase dramatically and the CFSv2 is gradually incapable of the

© 2016 The Authors. *International Journal of Climatology* published by John Wiley & Sons Ltd on behalf of the Royal Meteorological Society.

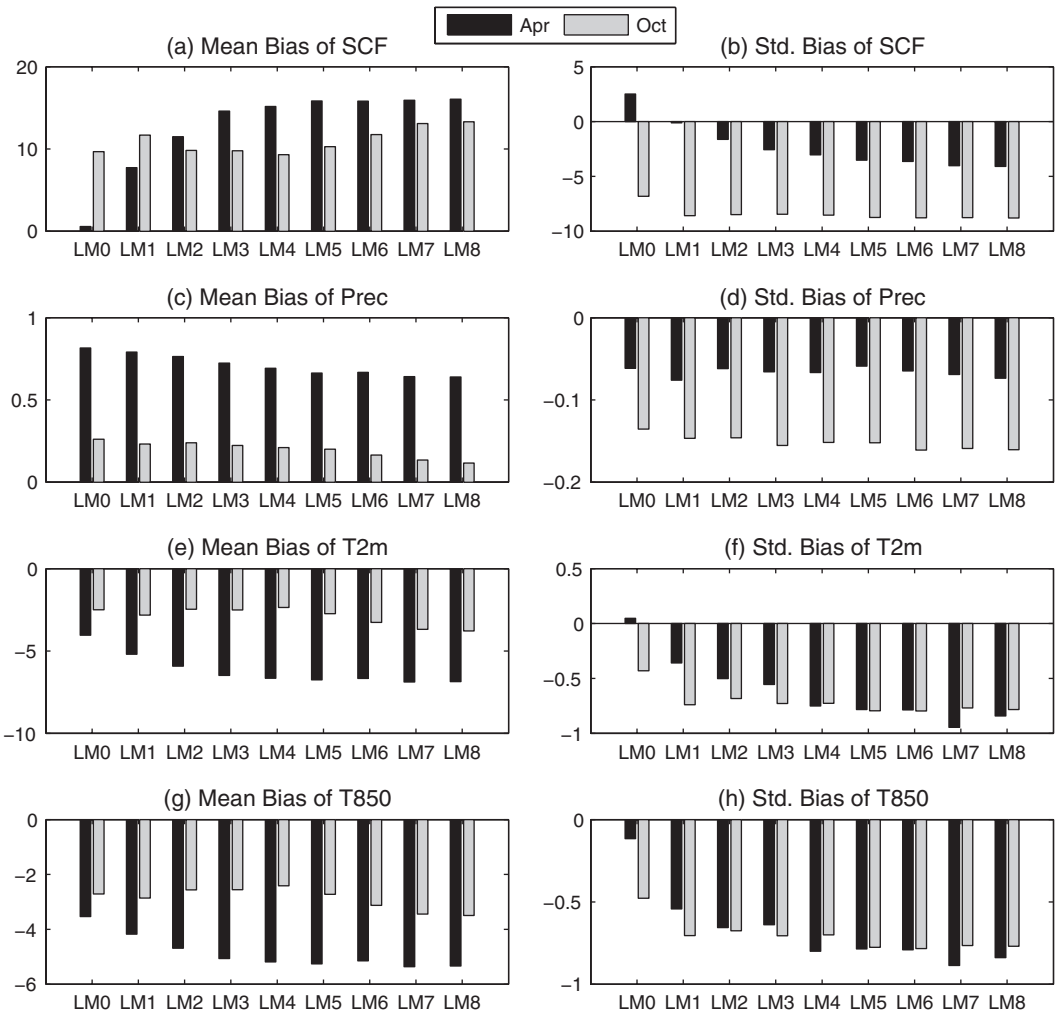

Figure 12. Mean biases (left panel) of (a) SCF (%), (c) Precipitation (mm-day^{-1}), (e) 2-m temperature (°C) and (g) 850 hPa temperature (°C) and their standard deviation biases (right panel, (b), (d), (f) and (h)) in April (black bar) and October (gray bar) for LM0-8.

interannual variation. Distinct from the snowmelt season, the biases in snowfall season vary little with the LM. The observed Eurasian SCF in October shows an upward tendency whereas the CFSv2 exhibits downward trends for all LMs. In addition, the CFSv2 simulates much weaker interannual variation compared with the observation. As a consequence, the CFSv2 is incapable of reproducing the leading pattern of Eurasian SCF in October. Overall, the CFSv2 exhibits a better predictive skill for Eurasian SCF in the snowmelt season than in the snowfall season except the climatological value. The predictive skills in both the snowmelt and snowfall season are abruptly improved and become much greater and stable after late-1990s than before. It is probably related with the change of snowpack initialization in 1997 in the model (Ek *et al.*, 2003; Saha *et al.*, 2010) and the higher temporal and spatial resolution product from 1997 which Rutgers observation bases on (Ramsay, 1998).

The model biases of SCF are strongly related with LTT and precipitation biases in both the snowmelt and snowfall seasons. The joint impact of the underestimated LTT and overestimated precipitation in the CFSv2 reasonably interprets the exaggerative SCF in the two seasons. Meanwhile, the CFSv2 simulates weaker variations of the LTT and precipitation in comparison with the observation generally, which may be the important factor for the underestimation of SCF interannual variability. The variability biases of precipitation in October and its relationship with SCF biases are more pronounced than those in April. In addition, the CFSv2 has poorer prediction skill in precipitation than LTT. As a result, the CFSv2 shows a worse predictive skill in the SCF interannual variation in October than in April.

The October SCF in the observation shows obvious upward trend while the forecasted October SCF in the CFSv2 for all LMs exhibits downward tendencies. Considering the important effect of the LTT and precipitation on the SCF in snowfall season, we further explore the tendency of October T2m, T850 and precipitation in the observation and the CFSv2. All these variables do not exhibit significant tendency (figure not shown). Therefore, one possible explanation is that the upward tendency in the observation is realistic whereas the CFSv2 is incapable of reproducing it. Assumed that the IC plays a dominant effect on the forecasted Eurasian SCF even after 9 months, the CFSv2, running from these IC with

© 2016 The Authors. *International Journal of Climatology* published by John Wiley & Sons Ltd on behalf of the Royal Meteorological Society.

decreasing trend, consequently predicts decreasing trend. In fact, the SCF in January–September from CFSR shows consistent decreasing tendency, which may account for the forecasted downtrend of October SCF in the CFSv2. However, we cannot exclude the possibility that the upward tendency in the observed Eurasian SCF is artificial. The coarse weekly product by trained NOAA meteorologists was officially replaced in the late 1990s with a daily Interactive Multisensor Snow and Ice Mapping System (IMS) product (http://climate.rutgers.edu/snowcover/), which may cause the abrupt increasing in late-1990s of Eurasian SCF in October. Using other four independent snow cover datasets, Brown and Derksen (2013) argued that the increasing trend of October snow cover from NOAA dataset is caused by the inconsistence of the mapping product. The features, especially the tendency, of snow cover in October deserve further investigation.

Acknowledgements

This study was jointly supported by the National Natural Science Foundation of China (41205059, 41221064 and 41375092), the National Basic Research Program of China (Grant 2014CB953900), the Special Fund for Public Welfare Industry (Meteorology) (GYHY201206017) and the Basic Research Fund of Chinese Academy of Meteorological Sciences (2015Z001).

References

Adler RF, Huffman GJ, Chang A, Ferraro R, Xie PP, Janowiak J, Rudolf B, Schneider U, Curtis S, Bolvin D, Gruber A, Susskind J, Arkin P, Nelkin E. 2003. The version 2 Global Precipitation Climatology Project (GPCP) monthly precipitation analysis (1979-present). *J. Hydrometeorol.* **4**: 1147–1167.

Barnett TP, Dümenil L, Schlese U, Roeckner E, Latif M. 1989. The effect of Eurasian snow cover on regional and global climate variations. *J. Atmos. Sci.* **46**: 661–686.

Berrisford P, Dee D, Fielding K, Fuentes M, Kållberg P, Kobayashi S, Uppala S, Simmons A. 2009. The ERA-Interim archive. Era Report Series 1, Technical Report, European Centre for Medium Range Weather Forecasts, Berkshire, UK, 23 pp.

Brands S, Manzanas R, Gutiérrez JM, Cohen J. 2012. Seasonal predictability of wintertime precipitation in Europe using the snow advance index. *J. Clim.* **25**(12): 4023–4028.

Brown RD, Derksen C. 2013. Is Eurasian October snow cover extent increasing? *Environ. Res. Lett.* **8**(2): 279–288, doi: 10.1088/1748-9326/8/2/024006.

Chen H, Duo Q, Bei X. 2013. Influence of snow melt anomaly over the mid–high latitudes of the Eurasian continent on summer low temperatures in northeastern China. *Chin. J. Atmos. Sci.* **37**(6): 1337–1347 (in Chinese).

Clark MP, Serreze MC. 2000. Effects of variations in East Asian snow cover on modulating atmospheric circulation over the North Pacific Ocean. *J. Clim.* **13**: 3700–3710.

Clark MP, Serreze MC, Robinson DA. 1999. Atmospheric controls on Eurasian snow extent. *Int. J. Climatol.* **19**: 27–40.

Cohen J, Jones J. 2011. A new index for more accurate winter predictions. *Geophys. Res. Lett.* **38**(21): 759–775.

Ek MB, Mitchell KE, Lin Y, Rogers E, Grunmann P, Koren V, Gayno G, Tarpley JD. 2003. Implementation of Noah land surface model advances in the National Centers for Environmental Prediction operational mesoscale Eta model. *J. Geophys. Res.* **108**: 8851, doi: 10.1029/2002JD003296.

Fan Y, van den Dool H. 2008. A global monthly land surface air temperature analysis for 1948–present. *J. Geophys. Res.* **113**: D01103, doi: 10.1029/2007JD008470.

Frei A, Miller JA, Robinson DA. 2003. Improved simulations of snow extent in the second phase of the Atmospheric Model Intercomparison Project (AMIP-2). *J. Geophys. Res.* **108**(D12): 975–984, doi: 10.1029/2002JD003030.

Gong G, Entekhabi D, Cohen J. 2003. Modeled Northern Hemisphere winter climate response to realistic Siberian snow anomalies. *J. Clim.* **16**: 3917–3931.

Hardiman SC, Kushner PJ, Cohen J. 2008. Investigating the ability of general circulation models to capture the effects of Eurasian snow cover on winter climate. *J. Geophys. Res.* **113**: D21123, doi: 10.1029/2008JD010623.

Hu Z-Z, Kumar A. 2014. Prediction skill of North Pacific variability in NCEP Climate Forecast System version 2: impact of ENSO and beyond. *J. Clim.* **27**(11): 4263–4272, doi: 10.1175/JCLI-D-13-00633.1.

Huang B. 2004. Remotely forced variability in the tropical Atlantic Ocean. *Clim. Dyn.* **23**(2): 133–152.

Kendall MG. 1975. Rank correlation methods. Charles Griffin, London.

Kim HM, Webster PJ, Curry JA. 2012. Seasonal prediction skill of ECMWF System 4 and NCEP CFSv2 retrospective forecast for the Northern Hemisphere winter. *Clim. Dyn.* **39**: 2957–2973, doi: 10.1007/s00382-012-1364-6.

Koren V, Schaake J, Mitchell K, Duan QY, Chen F, Baker JM. 1999. A parameterization of snowpack and frozen ground intended for NCEP weather and climate models. *J. Geophys. Res.* **104**(D16): 19569–19585.

Kug JS, Kang IS, Choi DH. 2008. Seasonal climate predictability with tier-one and tier-two prediction systems. *Clim. Dyn.* **31**: 403–416.

Kumar KK, Hoerling M, Rajagopalan B. 2005. Advancing Indian monsoon rainfall predictions. *Geophys. Res. Lett.* **32**: L08704, doi: 10.1029/2004GL021979.

Mann HB. 1945. Nonparametric test against trend. *Econometrica* **13**(3): 245–259.

Mo KC, Shukla S, Lettenmaier DP, Chen LC. 2012. Do climate forecast system (CFSv2) forecasts improve seasonal soil moisture prediction? *Geophys. Res. Lett.* **39**: L23703, doi: 10.1029/2012GL053598.

Orsolini YJ, Senan R, Balsamo G, Doblas-Reyes FJ, Vitart F, Weisheimer A, Carrasco A, Benestad RE. 2013. Impact of snow initialization on sub-seasonal forecasts. *Clim. Dyn.* **41**(7–8): 1969–1982, doi: 10.1007/s00382-013-1782-0.

Peng P, Barnston AG, Kumar A. 2013. A comparison of skill between two versions of the NCEP climate forecast system (CFS) and CPC's operational short-lead seasonal outlooks. *Weather Forecast.* **28**: 445–462.

Ramsay BH. 1998. The interactive multisensor snow and ice mapping system. *Hydrol. Processes* **12**: 1537–1546.

Riddle EE, Butler AH, Furtado JC, Cohen J, Kumar A. 2013. CFSv2 ensemble prediction of the wintertime Arctic Oscillation. *Clim. Dyn.* **41**: 1099–1116, doi: 10.1007/s00382-013-1850-5.

Robinson DA, Dewey KF, Heim RR. 1993. Global snow cover monitoring: an update. *Bull. Am. Meteorol. Soc.* **74**: 1689–1696.

Saha S, Moorthi S, Pan H-L, Wu X, Wang J, Nadiga S, Tripp P, Kistler R, Woollen J, Behringer D, Liu H, Chuang H, Juang HMH, Sela J, Iredell M, Treadon R, Kleist D, Delst PV, Keyser D, Derber J, Ek M, Meng J, Wei H, Yang R, Lord S, Dool HVD, Kumar A, Wang W, Long C, Chelliah M, Xue Y, Huang B, Schemm JK, Ebisuzaki W, Lin R, Xie PP, Chen MY, Zhou ST, Higgins W, Zou CZ, Liu Q, Chen Y, Han Y, Cucurull L, Reynolds RW, Rutledge G, Goldberg M. 2010. The NCEP climate forecast system reanalysis. *Bull. Am. Meteorol. Soc.* **91**: 1015–1057, doi: 10.1175/2010Bams3001.1.

Saha SK, Pokhrel S, Chaudhari HS. 2013. Influence of Eurasian snow on Indian summer monsoon in NCEP CFSv2 freerun. *Clim. Dyn.* **41**(7–8): 1801–1815, doi: 10.1007/s00382-01201617-4.

Saha S, Moorthi S, Wu X, Wang J, Nadiga S, Tripp P, Behringer D, Hou YT, Chuang H, Iredell M, Ek M, Meng J, Yang R, Mendez MP, van den Dool H, Zhang Q, Wang W, Chen M, Becker E. 2014. The NCEP Climate Forecast System version 2. *J. Clim.* **27**: 2185–2208, doi: 10.1175/JCLI-D-12-00823.1.

Singh KK, Mishra VD, Garg RK. 2007. Microwave response of seasonal snow-cover measured by using a ground-based radiometer at 6.93 and 18.7 GHz frequencies and at dual polarization. *J. Indian Soc. Remote Sens.* **35**(3): 243–251.

Venzke S, Allen MR, Sutton RT, Rowell DP. 1999. The atmospheric response over the North Atlantic to decadal changes in sea surface temperature. *J. Clim.* **12**: 2562–2584.

Wang B, Ding QH, Fu XH, Kang IS, Jin K, Shukla J, Doblas-Reyes F. 2005. Fundamental challenge in simulation and prediction of summer monsoon rainfall. *Geophys. Res. Lett.* **32**: L15711.

© 2016 The Authors. *International Journal of Climatology* published by John Wiley & Sons Ltd on behalf of the Royal Meteorological Society.

Wang W, Huang MP, Weaver SJ, Kumar A, Fu XH. 2012. MJO prediction in the NCEP Climate Forecast System version 2. *Clim. Dyn.* **42**(9–10): 2509–2520, doi: 10.1007/s00382-013-1806-9.

Wang W, Chen M, Kumar A. 2013. Seasonal prediction of Arctic Sea ice extent from a coupled dynamical forecast system. *Mon. Weather Rev.* **141**: 1375–1394, doi: 10.1175/MWR-D-12-00057.1.

Wu R, Kirtman BP. 2007. Observed relationship of spring and summer East Asian rainfall with winter and spring Eurasian snow. *J. Clim.* **20**(7): 1285–1304.

Wu B, Yang K, Zhang R. 2009. Eurasian snow cover variability and its association with summer rainfall in China. *Adv. Atmos. Sci.* **26**: 31–44.

Zhang R, Wu B, Zhao P, Han J. 2008. The decadal shift of the summer climate in the late 1980s over eastern China and its possible causes. *Acta Meteorol. Sin.* **22**: 435–445.

Zhang R, Wu B, Han J, Zuo Z. 2013. Effects on summer monsoon and rainfall change over China due to Eurasian snow cover and ocean thermal conditions. In *Climate Change – Realities, Impacts Over Ice Cap, Sea Level and Risks*, Singh BR (ed). InTech: Rijeka, Croatia, 227–250.

Zuo Z, Yang S, Wang W, Kumar A, Xue Y, Zhang R. 2011. Relationship between anomalies of Eurasian snow and southern China rainfall in winter. *Environ. Res. Lett.* **6**: 045402, doi: 10.1088/1748-9326/6/4/045402.

Zuo Z, Zhang R, Wu B. 2012a. Inter-decadal variations of springtime rainfall over southern China mainland for 1979–2004 and its relationship with Eurasian snow. *Sci. China Earth Sci.* **55**(2): 271–278.

Zuo Z, Zhang R, Wu B, Rong X. 2012b. Decadal variability in springtime snow over Eurasia: relation with circulation and possible influence on springtime rainfall over China. *Int. J. Climatol.* **32**(9): 1336–1345.

Zuo Z, Yang S, Hu ZZ, Zhang R, Wang W, Huang B, Wang F. 2013. Predictable patterns and predictive skills of monsoon precipitation in Northern Hemisphere summer in NCEP CFSv2 reforecasts. *Clim. Dyn.* **40**: 3071–3088, doi: 10.1007/s00382-013-1772-2.

Zuo Z, Yang S, Zhang R, Xiao D, Guo D, Ma L. 2014. Response of summer rainfall over China to spring snow anomalies over Siberia in the NCEP CFSv2 reforecast. *Q. J. R. Meteorol. Soc.* **141**: 939–944, doi: 10.1002/qj.2413.

© 2016 The Authors. *International Journal of Climatology* published by John Wiley & Sons Ltd on behalf of the Royal Meteorological Society.